

Article

The Effect of Magnitude M_w and Distance R_{rup} on the Fragility Assessment of a Multistory RC Frame Due to Earthquake-Induced Structural Pounding

Maria G. Flenga and Maria J. Favvata * 

Civil Engineering Department, University of Patras, 26504 Rio, Greece; mariaflenga@upnet.gr

* Correspondence: mfavvata@upatras.gr

Abstract: The effect of an intensity measure's (IM's) sufficiency property on the probabilistic assessment of reinforced concrete (RC) structures due to floor-to-floor structural pounding conditions is examined. In the first part of this investigation, efficiency and sufficiency properties of 23 scalar IMs are verified. Then, the magnitude M_w and the distance R_{rup} are examined as elements in a vector with an efficient scalar IM to evaluate whether they have any significant effect on the structural response. Subsequently, probabilistic seismic demand models (PSDMs) are developed using linear regression analyses based on a scalar IM and a vector-valued IM. Fragility curves are developed based on these PSDMs, and the influence of M_w and R_{rup} on the evaluation of the minimum required separation gap distance $d_{g,min}$ due to the pounding effect is examined. More than two hundred nonlinear time history analyses are performed based on the Cloud Analysis method. Seismic displacement demands that control of the global state of the structure, as well as the probability of structural pounding, are examined. The results of this research indicate that once M_w or R_{rup} is increased, fragility curves are shifted to greater values of IM, and the probability of the exceedance of a certain performance level is reduced. Also, the predictive power of R_{rup} seems to be greater than the one of M_w . On the other hand, it is revealed that M_w and R_{rup} induce variabilities in the demand solutions for adequate separation gap distance between the adjacent structures. Therefore, variation in M_w or R_{rup} may lead, in some cases, to unacceptable evaluations of the pounding effect in the capacity levels of structures.

Keywords: structural pounding; ground motion; efficiency property; sufficiency property; fragility curve; separation gap distance; Eurocode 8; nonlinear dynamic analysis; reinforced concrete structure



Citation: Flenga, M.G.; Favvata, M.J. The Effect of Magnitude M_w and Distance R_{rup} on the Fragility Assessment of a Multistory RC Frame Due to Earthquake-Induced Structural Pounding. *Buildings* **2023**, *13*, 1832. <https://doi.org/10.3390/buildings13071832>

Academic Editor: Magdalini D.

Titirila

Received: 2 July 2023

Revised: 14 July 2023

Accepted: 17 July 2023

Published: 20 July 2023



Copyright: © 2023 by the authors. Licensee MDPI, Basel, Switzerland. This article is an open access article distributed under the terms and conditions of the Creative Commons Attribution (CC BY) license (<https://creativecommons.org/licenses/by/4.0/>).

1. Introduction

Over the last three decades, numerous studies on the earthquake-induced pounding between adjacent buildings have been reported in the literature, while in recent years, a probabilistic assessment of the pounding risk has also been introduced and accepted [1].

Even in the case of base-isolated buildings where the superstructures are expected to remain linear elastic, the potential of pounding has been identified as a critical situation that can also lead to the unacceptable collapse probability of the structural elements [2].

Among different approaches, the fragility-based method is commonly used for the probabilistic evaluation of the seismic performance of structures. In this method, fragility curves are developed to accurately represent the probability of an Engineering Demand Parameter (EDP) exceeding a damage level for a given intensity measure (IM). For the needs of the statistical process, nonlinear dynamic analyses are performed to generate the samples of EDP | IM [3].

However, the reliability of the overall fragility assessment depends on the IM that has been selected to be used. In order to quantify the suitability of an IM, different criteria such as efficiency [4], sufficiency [5], proficiency, practicality [6], and hazard computability [7] have been proposed. Among them, the efficiency and sufficiency criteria are the most

examined IM properties in earthquake structural engineering. An IM is characterized as an efficient one if it predicts the structural response with small variability. Therefore, the uncertainties of record-to-record variability are reduced, and a small number of records can be used for performing nonlinear dynamic analyses. A sufficient IM indicates independence from ground motion parameters such as the magnitude M_w and the distance R_{rup} .

The literature provides several research studies that evaluate the correlation between IMs and EDPs [8–11]. However, only a few studies have focused on the verification of an appropriate IM when considering the earthquake-induced structural pounding phenomenon [12–17]. In this view, Tubaldi et al. [12] examined three different IMs regarding efficiency and sufficiency properties to assess the pounding risk of Single-Degree-Of-Freedom (SDOF) and Multi-Degree-Of-Freedom (MDOF) systems. The examined IMs arise as a modification of the spectral displacement IM. In 2016, Tubaldi et al. [13] examined the sufficiency of three different IMs based on the Relative Sufficiency Measure (RSM) and developed different types of regression models. For the probabilistic seismic assessment of the pounding effect between RC structures, Flenga and Favvata [14–16] examined the adequacy of the Peak Ground Acceleration (PGA) and the spectral acceleration at the first-mode period T_1 of the structure ($S_{a,T1}$) measures. Langlade et al. [17] examined the efficiency and the sufficiency of six different IMs in the structural pounding framework between two SDOF systems. Most of these results indicate that the efficiency of an IM is usually accompanied by a lack of sufficiency.

On the other hand, the fragility assessment of structures against pounding is based on traditional scalar IMs such as the PGA or $S_{a,T1}$ [1,12–16,18,19]. In this way, the uncertainties of the ground motions have not been comprehensively studied and, therefore, the degree of dispersion induced on the fragility analysis has not been evaluated in the framework of structural pounding. Recently, vector-valued IMs were proposed for use in the literature to demonstrate the predictive power of ground motion characteristics. These IMs may involve a traditional scalar IM with a second parameter that is associated with the characteristics of the ground motion [20,21]. For example, Baker and Cornell [20] studied the effect of epsilon when computing the drift hazard curve by using a vector-valued IM. Alternately, vector IMs consisting of multiple parameters can be used for improving the prediction of the structural response, for forecasting the EDPs in gravity dams, and for assessing the performance of isolated structures, bridges, or hydraulic tunnels [22–25]. Nevertheless, so far, vector IMs have not been used to capture the seismic performance of RC structures against pounding.

The objective of this study is to evaluate for the first time in the literature the effect of M_w and R_{rup} on the fragility assessment of multistory RC structures due to floor-to-floor structural pounding conditions. For this purpose, the concept of a vector-valued IM is utilized, while 23 scalar IMs are firstly evaluated to determine their adequacy in terms of efficiency and sufficiency properties. Then, new PSDMs and fragility curves are developed based on both scalar IMs and vector-valued IMs. The degree of variability induced on the probabilistic evaluation of the structural pounding due to M_w and R_{rup} is estimated. The assessment incorporates (a) the separation gap distance d_g between the adjacent structures; (b) the maximum interstory drift performances, IDR_{max} ($\%h_{st}$); and (c) the results of a compounded fragility-based solution that incorporates the separation distance (d_g) between the adjacent structures with the capacity level (performance level) of an EDP.

2. Case Study

In this work, an eight-story RC frame structure is considered to assess the fragility performance against pounding. The design of the frame is based on Eurocodes 2 and 8. The structure has three spans and a total height equal to 25.6 m. Each story has a height equal to 3.2 m, while the span's width is 6.0 m (Figure 1).

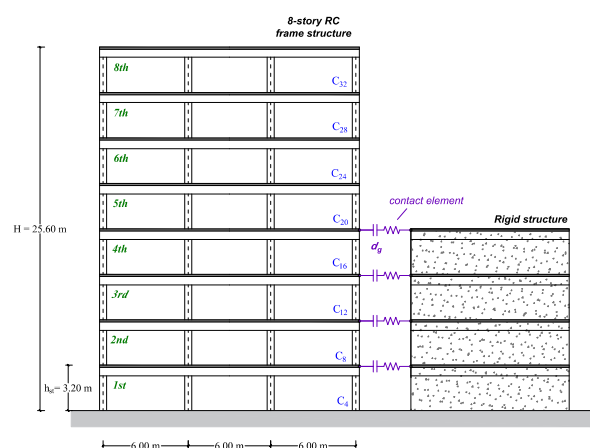


Figure 1. Examined RC frame subjected to floor-to-floor structural pounding.

To incorporate the structural pounding parameter, a rigid structure was deemed adjacent to the RC frame, so the top contact level was to be sited at the fourth floor (floor-to-floor pounding type). The use of an adjacent rigid structure indicates that the evaluation of the pounding effect was dependent only on the seismic demands of the tall and flexible RC frame [26]. Critical issues regarding the simulation of collisions between the adjacent structures are discussed in Flenga and Favvata [1]. A separation gap distance (d_g) equal to $d_g = 0.0$ cm (structures are in contact from the beginning) or $d_g = 2.0$ cm was examined. In total, two hundred ninety-four (294) nonlinear time history analyses were performed in the concept of the Cloud Analysis method [3] to define the samples of the EDPs as a function of the IMs. The generated pairs of EDP|IM depict the seismic performance in the case of free vibration of the eight-story RC frame as well as the corresponding responses in the case of structural pounding situation. For the correlation process, two displacement-based EDPs were examined: (a) the maximum displacement (δ_{max}) at the fourth-floor level, and (b) the maximum interstory drift as a function of the story height (IDR_{max} , $\%h_{st}$). The Drain-2dx program was used to perform the structural modeling and the non-linear dynamic analyses [27].

3. Ground Motions and Intensity Measures

Both horizontal components of forty-nine unscaled strong ground motions extracted from PEER's and ESM's databases were used [28,29]. All ground motions had a magnitude M_w greater than 5.5 and a distance R_{rup} greater than 9.60 km. All excitations were recorded on soils with average shear wave velocity, $v_{s,30}$, which was up to 813.5 m/s (soil class A in EC8). Table 1 shows the characteristics of the adopted seismic records. It is noted that all the records used in this study do not contain velocity pulses. However, it has been shown that near-fault ground motions with velocity pulses may significantly influence the seismic performance of the structures [30]. In these types of seismic records, structures exhibit larger displacements and velocities and, therefore, in the case of pounding with an adjacent structure, impact forces are increased, and greater damages are expected to be caused [30].

Table 1. Ground motions.

No.	Earthquake ID	Earthquake Name	Station Name	Magnitude M_w	Distance R_{rup} (km)	Duration (s)	No.	Earthquake ID	Earthquake Name	Station Name	Magnitude M_w	Distance R_{rup} (km)	Duration (s)
1	RSN 643	Whittier Narrows-01	LA—Wonderland Ave	5.99	27.64	18.14	26	EMSC-20161030_0000029	Central Italy	Teramo	6.50	27.87	61.38
2	RSN 4312	Umbria-03, Italy	Gubbio	5.60	15.72	17.99	27	ME-1979-0003	Northwestern Balkan Peninsula	Hercegnovi Novi-O.S.D. Pavicic School	6.90	24.00	47.96
3	IT-2009-0009	L' Aquila	Monte Reale	6.10	17.11	99.99	28	RSN 5618	Iwate, Japan	IWT010	6.90	16.27	237.99
4	EMSC-20160824_0000006	Central Italy	Teramo	6.00	22.12	78.61	29	RSN 1091	Northridge-01	Vasquez Rocks Park	6.69	23.64	39.98
5	IT-1984-0004	Lazio Abruzzo	Atina	5.90	16.32	30.68	30	RSN 3954	Tottori, Japan	SMNH10	6.61	15.59	299.99
6	RSN 680	Whittier Narrows-01	Pasadena—CIT Kresge Lab	5.99	18.12	39.99	31	EMSC-20161030_0000029	Central Italy	Reggiano	6.50	21.27	61.38
7	GR-1999-0001	Greece	(ATH4)	5.90	16.79	42.35	32	ME-1979-0003	Northwestern Balkan Peninsula	Dubrovnik-Pomorska Skola	6.90	64.87	33.57
8	IT-2009-0009	L' Aquila	Antrodoco	6.10	23.18	120.00	33	RSN 284	Iprinia, Italy	Auletta	6.90	9.60	34.00
9	EMSC-20170118_0000034	Central Italy	Leonessa	5.50	22.40	59.90	34	RSN 5006	ChuetsuJapan	FKSH07	6.80	79.54	158.99
10	IT-1997-0006	Umbria March	Monte Fiegni	6.00	21.98	34.75	35	RSN 5993	El Mayor-Cucapah	El Monte County Park	7.20	104.9	154.84
11	RSN 4438	Molise-02, Italy	Sannicandro	5.70	51.32	36.28	36	RSN 3799	Hector Mine	LA—Griffith Park Observatory	7.13	185.92	56.99
12	RSN 1649	Sierra Madre	Vasquez Rocks Park	5.61	39.81	39.98	37	RSN 788	Loma Prieta	Piedmont Jr High School Grounds	6.93	73.00	39.99
13	IT-2012-0008	Emilia 1st shock	S Zeno Di Montagna	6.10	77.86	200.00	38	RSN 4167	Niigata, Japan	FKSH07	6.63	52.3	179.99
14	EMSC-20161026_0000095	Central Italy	Monte Murano	5.90	48.95	124.81	39	RSN 804	Loma Prieta	So. San Francisco, Sierra Pt.	6.90	63.10	25.00
15	RSN 2805	Chi-Chi Taiwan-04	KAU003	6.20	116.20	60.00	40	RSN 59	San Fernando	Cedar Springs, Allen Ranch	6.60	89.70	14.00
16	ME-1979-0012	Northwestern Balkan Peninsula	Hercegnovi Novi-O.S.D. Pavicic School	6.20	30.7	24.58	41	RSN 283	Iprinia, Italy	Arienzo	6.90	52.90	24.00
17	RSN8168	Parkfield-02, CA	Diablo Canyon Power Plant	6.00	78.32	39.67	42	RSN 5363	Chuetsu-oki, Japan	TCGH17	6.80	102.41	237.99
18	GR-1997-0019	Ionian Sea	Kyparissia	6.40	104.34	27.80	43	RSN 6041	El Mayor-Cucapah	San Diego Road Dept	7.20	110.95	163.68
19	IT-2012-0008	Emilia 1st shock	Tregnago	6.10	63.89	160.18	44	RSN 5483	Iwate, Japan	AKTH05	6.90	39.41	177.99
20	EMSC-20161026_0000095	Central Italy	Teramo	5.90	41.70	187.49	45	RSN 8167	San Simeon, CA	Diablo Canyon Power Plant	6.52	37.92	29.44
21	RSN 3479	Chi-Chi Taiwan-06	TCU085	6.30	83.40	42.00	46	RSN 4248	Niigata, Japan	TCGH17	6.63	77.50	295.99
22	RSN 2508	Chi-Chi Taiwan-03	CHY102	6.20	60.36	60.99	47	RSN 1245	Chi-Chi, Taiwan	CHY102	7.62	37.22	89.99
23	RSN 80	San Fernando	Pasadena—Old Seismo Lab	6.61	21.50	101.10	48	RSN 1257	Chi-Chi, Taiwan	HWA003	7.62	56.14	64.99
24	RSN 1011	Northridge-01	LA—Wonderland Ave	6.69	20.29	29.98	49	RSN 2107	Denali, Alaska	Carlo (temp)	7.90	50.90	60.00
25	RSN 3925	Tottori, Japan	OKYH07	6.61	15.23	299.99							

Thereafter, for each seismic record, twenty-three IMs were considered and numerically estimated (Table 2). The seismic IMs were either structural independent or structural dependent. The structural independent IMs were calculated directly from the time history of the examined ground motions and describe characteristics such as amplitude, duration, and frequency in terms of acceleration, velocity, or displacement [31–40].

Table 2. Examined intensity measures.

	IMs	Units	Name	Formula	Ref.
Structural Independent IMs					
<i>Acceleration-based</i>	PGA	[m/s ²]	Peak Ground Acceleration	$PGA = \max a(t) $	[31]
	RMS _a	[m/s ²]	Root-Mean-Square of Acceleration	$RMS_a = \sqrt{\frac{1}{T_d} \int_0^{T_d} (a(t))^2 dt}$	[34]
	I _a	[m/s]	Arias Intensity	$I_a = \int_0^{T_d} (a(t))^2 dt$	[35]
	I _c	-	Characteristic Intensity	$I_c = a_{rms}^{1.5} T_d^{0.5}$	[36]
	CAV	[m/s]	Cumulative Absolute Velocity	$CAV = \int_0^{t_{tot}} a(t) dt$	[32]
	SMA	[m/s ²]	Sustained Maximum Acceleration	3rd largest peak in acceleration time history	[33]
	EDA	[m/s ²]	Effective Design Acceleration	Peak acceleration value after filtering out time history above 9 Hz	[32]
	A ₉₅	[m/s ²]	A ₉₅ Parameter	The acceleration level below which 95% of the total Arias intensity is contained	[38]
<i>Velocity-based</i>	PGV	[m/s]	Peak Ground Velocity	$PGV = \max v(t) $	[31]
	RMS _v	[m/s]	Root-Mean-Square of Velocity	$RMS_v = \sqrt{\frac{1}{T_d} \int_0^{T_d} (v(t))^2 dt}$	[34]
	SED	[m/s ²]	Specific Energy Density	$SED = \int_0^{T_d} (v(t))^2 dt$	[31]
	SMV	[m/s]	Sustained Maximum Velocity	3rd largest peak in velocity time history	[33]
	MIV	[m/s]	Maximum Incremental Velocity	Maximum area under the acceleration curve between two zero crossings of the accelerogram	[37]
<i>Displacement-based</i>	PGD	[m]	Peak Ground Displacement	$PGD = \max d(t) $	[31]
	RMS _d	[m]	Root-Mean-Square of Displacement	$RMS_d = \sqrt{\frac{1}{T_d} \int_0^{T_d} (d(t))^2 dt}$	[34]
	PGV/PGA	[s]	Peak velocity to acceleration ratio	$PGV/PGA = \max v(t) /\max a(t) $	[31]
Structural Dependent IMs					
<i>Spectral</i>	S _{a,T1}	[m/s ²]	Spectral Acceleration S _a at the fundamental period T ₁ of the structure		[31]
	S _{v,T1}	[m/s]	Spectral Velocity S _v at the fundamental period T ₁ of the structure		[31]
	S _{d,T1}	[m]	Spectral Displacement S _d at the fundamental period T ₁ of the structure		[31]
<i>Integral</i>	ASI	[m/s]	Acceleration Spectrum Intensity	$ASI = \int_{0.1}^{0.5} S_a(0.05, T) dT$	[39]
	VSI	[m]	Velocity Spectrum Intensity	$VSI = \int_{0.1}^{2.5} S_v(0.05, T) dT$	[39]
	HI	[m]	Housner Intensity	$HI = \int_{0.1}^{2.5} PSV(0.05, T) dT$	[41]
<i>Multi param.</i>	S _{a,avg}	[m/s ²]	Average Spectral Acceleration	$S_{a(T1...TN)} = \left(\prod_{i=1}^n S_a(T_i) \right)^{1/n}$	[42]

On the other hand, the structural dependent IMs were evaluated using the response spectra of the ground motions and were classified as spectral, integral, and multi-parameter measures [8,31,41,42].

4. IMs' Efficiency and Sufficiency Properties

The seismic probabilistic assessment of a structure implies the use of IMs that verify specific criteria of efficiency and sufficiency. An efficient IM denotes that the variation in estimating the structural demand is small, while a sufficient IM is independent of ground motion characteristics (M_w , R_{rup}).

Efficiency property: The most common method to evaluate the variability of an IM is through the logarithm standard deviation, $\beta_{EDP|IM}$. For this purpose, nonlinear dynamic analyses followed by linear regression of the estimated EDP | IM pairs in log-log space were performed. Adopting lognormal distribution for the structural demand [4], the $\beta_{EDP|IM}$ was calculated as:

$$\beta_{EDP|IM} = \sqrt{\frac{\sum_{i=1}^n (\ln EDP_i | IM_i - \ln \widehat{EDP} | IM)^2}{n - 2}} \quad (1)$$

where n is the number of the nonlinear dynamic analyses, and \widehat{EDP} is the median structural demand. Based on Mollaioli et al. [9], values of dispersion lower than 0.30 indicate ideal efficiency of the seismic intensity measure; however, a logarithm standard error in the range of 0.30–0.40 is also acceptable to characterize an IM as efficient.

Sufficiency property: The sufficiency of an IM is usually verified through the p -value between the residuals $\varepsilon|IM$ of the regression analysis and the examined characteristic of the ground motion (M_w or R_{rup}). In general, the p -value represents the probability of rejecting the null hypothesis ($H_0 = 0$), which states that the regression coefficient is zero. A p -value less than 0.05 (95% confidence level) indicates the insufficiency of the IM, while the regression coefficient is statistically significant. The p -value criterion evaluates the sufficiency property of an IM in an absolute sense. However, it is difficult to satisfy the sufficiency of a scalar IM since it requires the independence of all possible values of the IM from the examined ground motion characteristics [43]. Jalayer et al. [43] introduced the concept of the Relative Sufficiency Measure (RSM) to quantify the prediction capability of an IM instead of the reference IM for a certain EDP. The evaluation of the RSM is based on relative entropy and measures the similarity of two probability density functions (e.g., $p(EDP | IM_i)$ and $p(EDP | IM_j)$). The RSM can be approximately calculated for a suite of n ground motion using the following expression [43]:

$$I(EDP|IM_2|IM_1) \approx \frac{1}{n} \sum_{i=1}^n \log_2 \left(\frac{\beta_{EDP|IM_1} \Phi \left(\frac{\ln EDP_i - \ln \widehat{EDP} | IM_{2,i}}{\beta_{EDP|IM_2}} \right)}{\beta_{EDP|IM_2} \left(\frac{\ln EDP_i - \ln \widehat{EDP} | IM_{1,i}}{\beta_{EDP|IM_1}} \right)} \right) \quad (2)$$

where IM_1 is the reference and IM_2 is the candidate IM. In general, the RSM method quantifies the amount of information gained or lost in the case of using IM_2 instead of IM_1 . Positive values of $I(EDP|IM_2|IM_1)$ indicate that IM_2 is more sufficient than IM_1 , while negative values imply that IM_2 is less sufficient than IM_1 . Therefore, in this study, the sufficiency of a scalar IM was evaluated based on (a) the p -value of the regression analysis and (b) the RSM method.

5. Probabilistic Seismic Demand Model for Developing a Fragility Curve

A PSDM was developed based on pairs of EDP | IM that were extracted via nonlinear dynamic analyses of the structure. The mathematical relation between the \widehat{EDP} and the IM was then approximated using a two-parameter power law model as follows [3,4]:

$$\widehat{EDP} | IM = \alpha IM^b \quad (3)$$

where α and b are deduced based on the linear regression analysis of the logarithm IM and EDP. Therefore, Equation (3) can be written as:

$$\ln \text{EDP} | \text{IM} = b \ln \text{IM} + \ln \alpha + \varepsilon | \text{IM} \quad (4)$$

$\varepsilon | \text{IM}$ is the random error with mean zero and standard deviation β .

Following the aim of this study, the magnitude M_w and the distance R_{rup} were examined as elements in a vector with a scalar IM. In this case, the PSDM can be expressed as [4]:

$$\widehat{\text{EDP}} | \text{IM} = a \text{IM}^b e^{c M_w} R_{rup}^d \quad (5a)$$

or

$$\ln \text{EDP} | \text{IM} = \ln a + b \ln \text{IM} + c M_w + d \ln R_{rup} + \varepsilon | \text{IM} \quad (5b)$$

where a , b , c , and d are the regression analysis coefficients.

Since M_w or R_{rup} were examined as elements separately in a vector with a scalar IM, Equation (5b) is herein considered as follows:

$$\ln \text{EDP} | \text{IM} = \ln a + b \ln \text{IM} + c M_w + \varepsilon | \text{IM} \quad (6a)$$

$$\ln \text{EDP} | \text{IM} = \ln a + b \ln \text{IM} + d \ln R_{rup} + \varepsilon | \text{IM} \quad (6b)$$

Then, the fragility curve is defined by the closed-form solution as [3]:

$$G_{\text{EDP} | \text{IM}}(C | \text{IM}) = P[\text{EDP} | \text{IM} \geq C | \text{IM}] = \Phi \left(\frac{\ln \widehat{\text{EDP}} | \text{IM} - \ln \hat{C}}{\beta_{\text{EDP} | \text{IM}}} \right) \quad (7)$$

$\Phi(\cdot)$ is the standard normal cumulative function, \hat{C} is the median value of the capacity, and $\beta_{\text{EDP} | \text{IM}}$ is the logarithm standard deviation.

6. Results

6.1. Verification of IMs' Properties

In Figure 2, the results of the estimated $\beta_{\text{EDP} | \text{IM}}$ are presented to evaluate the IMs' efficiency property on the maximum demands of the eight-story RC frame in terms of (a) the displacement at fourth-floor level (δ_{\max}) and (b) the overall interstory drift ($\text{IDR}_{\max} - \%h_{st}$). In general, values of $\beta_{\text{EDP} | \text{IM}}$ lower than 0.40 indicate the superiority of an IM to predict the EDPs with reduced variation. Therefore, based on the results in Figure 2, except for the ASI, all the other structural dependent IMs can be characterized as efficient ones. On the contrary, the structural independent IMs show an increased variation in the prediction of the examined EDPs. In these cases, the structural independent IMs had values of $\beta_{\text{EDP} | \text{IM}}$ greater than 0.4. Nevertheless, among all the structural independent IMs, PGV and MIV showed better predictive capability to EDPs. The acceleration-based (including PGA) and the displacement-based structural independent IMs were the least effective, with PGV/PGA being the most invalid one. Furthermore, the evaluation of the IMs' efficiency seemed not to be affected when the structural pounding problem was involved. For example, the estimated values of $\beta_{\text{IDR}_{\max} | \text{IM}}$ were slightly increased when $d_g = 0.0$ cm in comparison with the cases of $d_g = 2.0$ cm or without pounding (Figure 2b). Additionally, the dispersion remained within the acceptable range ($\beta_{\text{IDR}_{\max} | \text{IM}} < 0.4$) for the structural dependent IMs.

Figure 3a shows the results of the IMs' sufficiency with respect to M_w and R_{rup} in the case of δ_{\max} . Results indicate that the structural dependent IMs (except ASI) were independent of M_w (blue line) (p -value > 0.05). Among the acceleration-based IMs, only I_a , I_c , and CAV satisfied the criterion of sufficiency, and that may be attributed to the fact that these IMs were characterized by the duration, the amplitude, and the frequency of the ground motion. The velocity-based and the displacement-based independent IMs were also independent of M_w , except for MIV and SED.

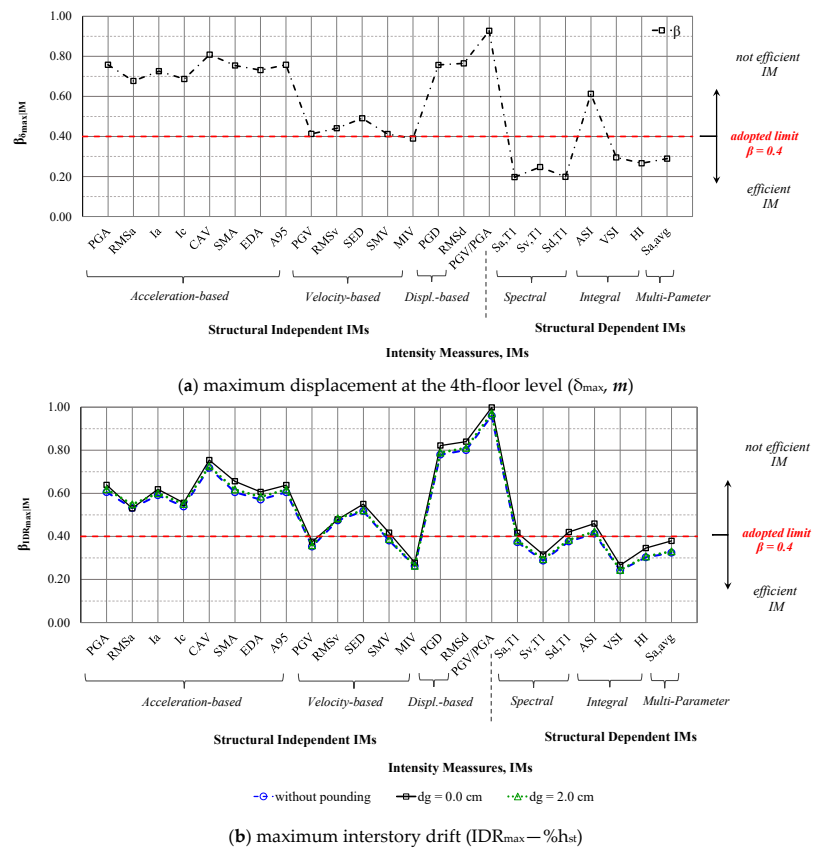


Figure 2. Evaluation of the IMs' efficiency— $\beta_{EDP|IM}$.

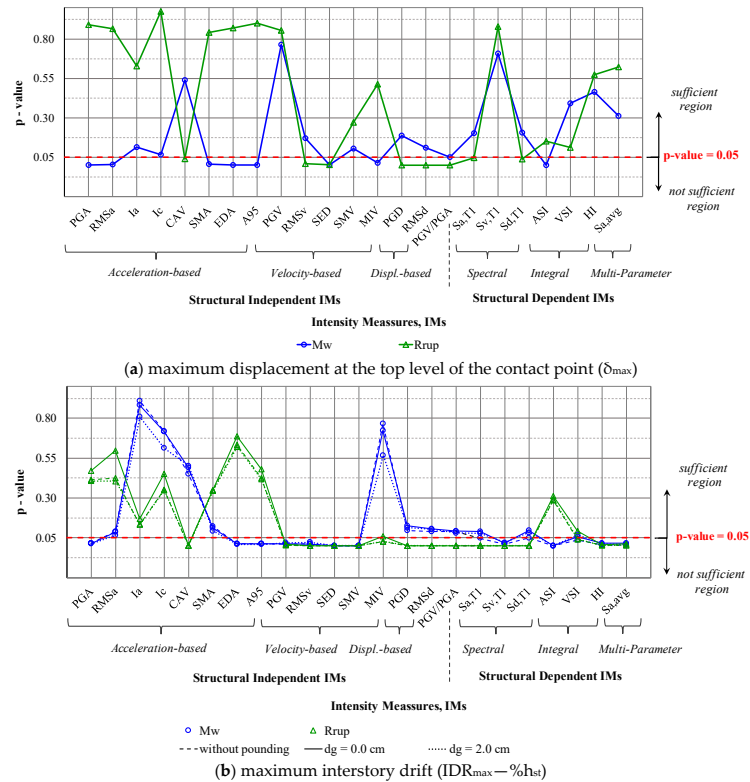


Figure 3. Evaluation of IMs' sufficiency for M_W and R_{Rup} .

Rating the IMs' sufficiency with respect to R_{rup} , the structural dependent IMs and the acceleration-based IMs were deduced to be independent (Figure 3—green line), since the p -values were greater than 0.05. The velocity-related IMs (except for RMS_v and SED) were more sufficient than the displacement-based IMs. Additionally, the structural independent PGV , SMV , I_a , and I_c were simultaneously independent of M_w and R_{rup} .

In Figure 3b, the evaluation of the IMs' sufficiency in terms of IDR_{max} for all the examined structural pounding cases is presented. As can be observed, the p -values of the structural dependent IMs and the p -values of the velocity-based PGV , RMS_v , SED , and SMV were around the limit value of 0.05 both for M_w and R_{rup} . However, the acceleration-based IMs of RMS_a , I_a , and I_c , seem to be the most sufficient IMs for the IDR_{max} demands of the eight-story structure with respect to the ground motion characteristics.

Furthermore, these results show that the pounding effect does not significantly alter the evaluation of the sufficiency property (Figure 3). In fact, similar p -values were estimated either with or without accounting for the structural pounding effect. When the separation gap distance was $d_g = 0.0$ cm, p -values with respect to R_{rup} (green lines) were slightly shifted to higher values for some IMs.

The above results (Figures 2 and 3) indicate that the satisfaction of the IMs' sufficiency implies a lack of the IMs' efficiency, and vice versa. For instance, the seismic measures I_a and I_c , which are independent of M_w and R_{rup} , did not pass the efficiency requirements since $\beta_{EDP|IM}$ was greater than the acceptable limit. However, the more efficient IMs ($\beta_{EDP|IM} < 0.4$) were more or less insufficient on the ground motion characteristics. Therefore, the IMs' sufficiency is further evaluated based on the RSM. $S_{a,T1}$ is examined since (a) it is the most common IM used in structural engineering, (b) it passes the efficiency property in both examined EDPs (δ_{max} , IDR_{max}), and (c) its p -values are shifted close to 0.05.

Therefore, in Figure 4, the relative sufficiency of the $S_{a,T1}$ with respect to the other IMs is presented. Demands in terms of δ_{max} and IDR_{max} were involved considering the examined distances (d_g). In the case of δ_{max} , the intensity measure $S_{a,T1}$ provided more information than the other IMs, while it was equally sufficient with $S_{d,T1}$.

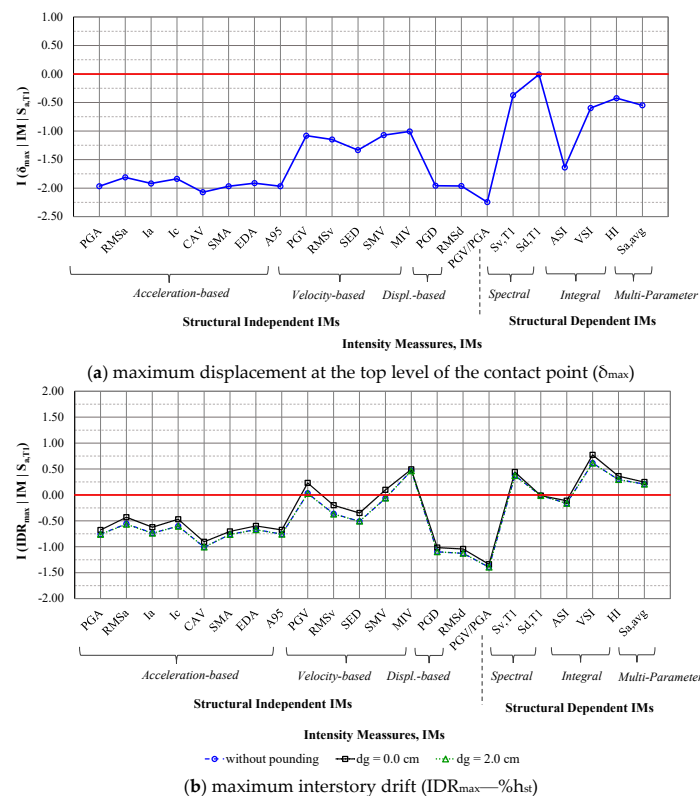


Figure 4. Sufficiency of the $S_{a,T1}$ relative to the other IMs—RSM method.

For example, the SMA was insufficient compared with the $S_{a,T1}$ since it provided 1.967 times less information regarding the demand δ_{max} (Figure 4a). Evaluating the relative sufficiency in the case of IDR_{max} , it can be observed that the structural dependent IMs (except ASI) provided more information than $S_{a,T1}$ (Figure 4b). Thus, $S_{a,T1}$ was more sufficient in a relative sense than the examined independent IMs, but it was insufficient with respect to the other structural dependent IMs. Finally, the RSM was slightly moved towards higher values when considering the pounding effect and $d_g = 0.0$ cm (Figure 4b) in comparison with the corresponding values without pounding. In the case of $d_g = 2.0$ cm, the RSMs were less than the ones depicted on the free vibration of the eight-story RC frame.

6.2. Probabilistic Assessment of Structural Pounding

In order to evaluate whether M_w or R_{rup} had any significant effect on the structure's fragility, they were examined as elements in a vector with a scalar IM (Section 5). Therefore, in this section, the $S_{a,T1}$ was considered as the scalar IM to examine the bias introduced due to its dependency on both M_w and R_{rup} . The choice of $S_{a,T1}$ was driven by its superiority in the efficiency property since (a) in the case of δ_{max} , it was the most efficient IM, and (b) in the case of IDR_{max} , the efficiency criterion was also covered. Further, as has already been mentioned, $S_{a,T1}$ was the most common IM used in structural engineering, while in most examined cases in this study, p -values were close to 0.05 (meaning limited sufficiency).

Therefore, new PSDMs considering the scalar $S_{a,T1}$ as well as the vector-valued $S_{a,T1}$ conditional to M_w or R_{rup} were defined. In Table 3, the PSDMs and the corresponding logarithm standard deviation $\beta_{EDP|IM}$ are presented.

Table 3. PSDMs using scalar and vector-valued IM.

EDP IM	$d_g^{(1)}$ [cm]	IM ⁽²⁾	$\ln \hat{EDP} = b \ln IM + c M_w + d \ln R_{rup} + a$	$\beta_{EDP IM}$
$IDR_{max} S_a$	0.0	Scalar	$\ln IDR_{max} = 0.835 \ln S_a + 1.256$	0.416
		Vector-valued	$\ln IDR_{max} = 0.867 \ln S_a - 0.16 M_w + 2.411$	0.410
			$\ln IDR_{max} = 0.766 \ln S_a - 0.252 \ln R_{rup} + 1.928$	0.387
	2.0	Scalar	$\ln IDR_{max} = 0.821 \ln S_a + 1.038$	0.381
		Vector-valued	$\ln IDR_{max} = 0.850 \ln S_a - 0.151 M_w + 2.129$	0.375
			$\ln IDR_{max} = 0.749 \ln S_a - 0.263 \ln R_{rup} + 1.740$	0.345
WP ⁽³⁾	WP ⁽³⁾	Scalar	$\ln IDR_{max} = 0.810 \ln S_a + 0.988$	0.373
		Vector-valued	$\ln IDR_{max} = 0.842 \ln S_a - 0.167 M_w + 2.189$	0.365
			$\ln IDR_{max} = 0.738 \ln S_a - 0.264 \ln R_{rup} + 1.693$	0.335
$\delta_{max} S_a$	WP ⁽³⁾	Scalar	$\ln \delta_{max} = 0.890 \ln S_a - 1.797$	0.197
		Vector-valued	$\ln \delta_{max} = 0.901 \ln S_a - 0.057 M_w - 1.387$	0.196
			$\ln \delta_{max} = 0.869 \ln S_a - 0.076 \ln R_{rup} - 1.595$	0.192

⁽¹⁾ d_g : separation gap distance, ⁽²⁾ IM: intensity measure, ⁽³⁾ WP: without pounding.

Thereafter, the fragility curves were developed. Specifically, in Figures 5 and 6, the scalar-based fragilities of the RC frame are presented with red lines, while the dashed lines depict the corresponding curves in the case of using a vector-valued $S_{a,T1}$ conditional to M_w or R_{rup} . The presented results are for (i) $d_g = 0.0$ cm, (ii) $d_g = 2.0$ cm, and (iii) without the pounding effect.

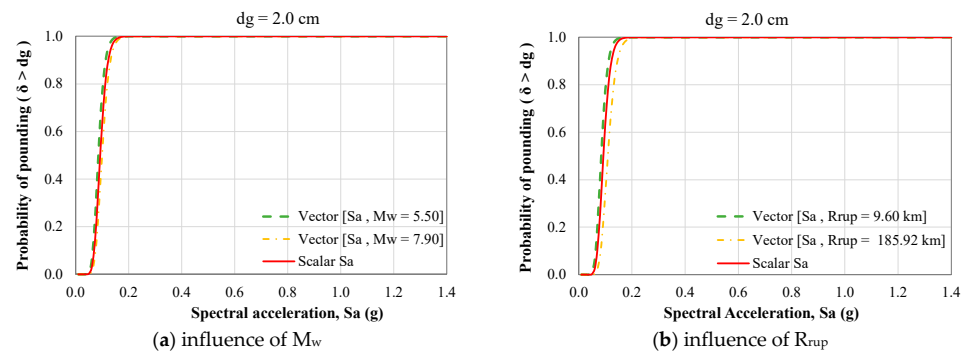


Figure 5. Influence of M_w and R_{rup} on assessing the probability of pounding when $d_g = 2.0$ cm. Fragility curves in terms of $S_{a,T1} | \delta_{max}$.

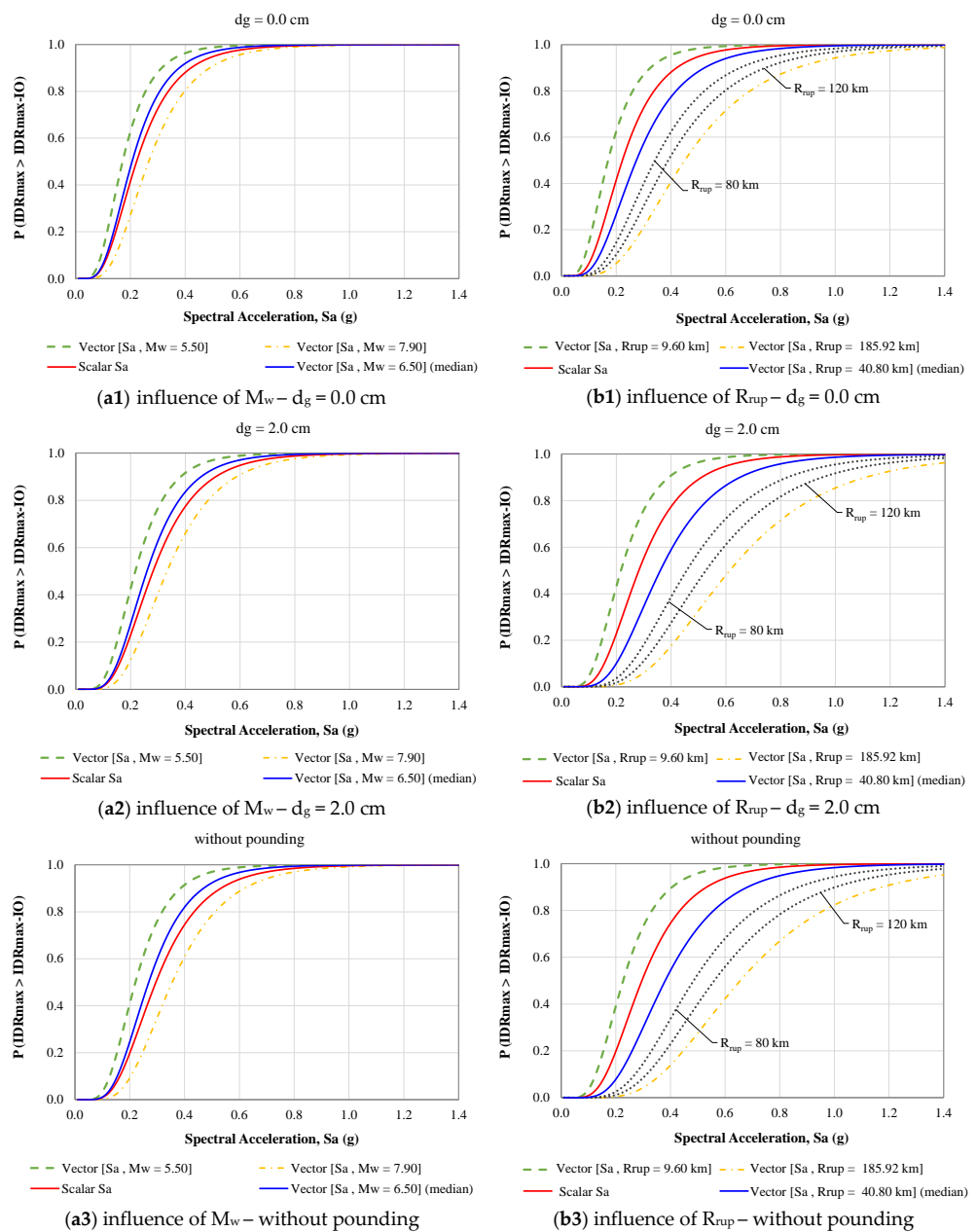


Figure 6. Influence of M_w (a) and R_{rup} (b) on the fragility assessment of the 8-story RC frame in terms of $S_{a,T1} | IDR_{max} (\%h_{st})$. Fragility curves at the performance level of Immediate Occupancy (IO) when: $d_g = 0.0$ cm (1), $d_g = 2.0$ cm (2), and without pounding (3).

Figure 5 shows results regarding the probability of pounding at different d_g between the adjacent structures. It can be observed that the outcomes of the assessment are independent with respect to M_w and R_{rup} when $d_g = 2.0$ cm.

In Figure 6, the influence of M_w and R_{rup} on the fragility of the eight-story RC structure in terms of IDR_{max} is presented. The IDR_{max} demand parameter was evaluated at the performance level of IO. Also in Figure 6, fragilities based on the median values of M_w and R_{rup} are presented. It is noted that, for the selected ground motions, M_w values ranged between 5.5 and 7.9, while values of R_{rup} were between 9.6 km to 185.92 km, and thus the median values of M_w and R_{rup} were 6.5 and 40.8 km, respectively. It can be observed that when M_w or R_{rup} is increased, fragility curves were shifted to greater values of $S_{a,T1}$, while the probability of exceedance of the performance level of IO was reduced for a specified value of $S_{a,T1}$. Nevertheless, the variation in the results was more pronounced when R_{rup} was involved, and the corresponding results deduced more conservatively when $S_{a,T1}$ was used as a scalar IM.

The vector-based fragility curve that depicted the median value of M_w (i.e., $M_w = 6.5$ —blue line) was slightly more conservative than the corresponding scalar-based fragility curve (red line) (Figure 6a). In the case of R_{rup} , the scalar-based fragility curve (red line) was shifted to lower values of $S_{a,T1}$ in comparison with the vector-based fragility curve that depicts the median value of R_{rup} (i.e., $R_{rup} = 40.8$ km—blue line) (Figure 6b). Similar observations also hold when the probability of pounding is evaluated at a d_g greater than 2.0 cm. Therefore, it can be stated that the fragility assessment of the structure based on the scalar $S_{a,T1}$ yields similar results as the assessment that is based on the vector-valued $S_{a,T1}$ conditional to median values of M_w and R_{rup} .

Regarding the effect of pounding on the probabilistic seismic assessment of the structure, the following key issues were noted (Figures 5 and 6): (a) the vulnerability of the structure in IDR_{max} at the performance level of IO was increased due to the structural pounding condition since the corresponding fragility curves were shifted to lower values of intensity in comparison with the free vibration mode, and (b) the initial separation gap distance between the adjacent structures altered the results of the assessment.

Recently, a compounded fragility-based method for the evaluation of the structural pounding effect on the performance of an RC structure was introduced by Flenga and Favvata [1] based on specified capacity levels of the examined EDPs and the available separation gap distances d_g between the adjacent structures. The implementation of this method introduces certain thresholds that identify the adequate value of d_g for minimizing the effect of pounding at a given performance level (local or/and global). More details can be found in Flenga and Favvata [1].

The fragility curves presented in Figure 7 describe the probability of pounding between the eight-story RC frame and the adjacent rigid structure at the fourth-floor level when $d_g = 0.0$ cm and $d_g = 2.0$ cm, while the case without pounding is also shown. On each fragility curve, characteristic points are depicted with dots (denoted as IM_L-P in the proposed method [1]). These points indicate the probability of pounding (P) at which the corresponding value of IM_L causes the exceedance of the IO performance level at the examined separation gap distance d_g . In the case of considering the scalar IM of $S_{a,T1}$, the corresponding IM_L-P points are shown with rhombus dots.

Taking into account the low values of M_w and R_{rup} (i.e., 5.5 and 9.6 km, respectively), rectangular dots are used to indicate the IM_L-P points based on the vector-valued IM ($[S_{a,T1}, M_w]$ or $[S_{a,T1}, R_{rup}]$). The triangle dots indicate the IM_L-P points based on the vector-valued $S_{a,T1}$ conditional to the highest recorded values of M_w and R_{rup} (i.e., 7.9 and 185.92 km, respectively). Finally, in Figure 7, the dashed lines that connect the characteristic data points IM_L-P among the examined d_g distances represent the so-called performance level thresholds in the case of the vector-valued IM of $[S_{a,T1}, M_w]$ or $[S_{a,T1}, R_{rup}]$, while the solid black line indicates the corresponding threshold in the case scalar intensity $S_{a,T1}$. In this way, the threshold line at the performance level of IO specifies the minimum demand for separation gap distance ($d_{g,min}$) at a given probability of pounding.

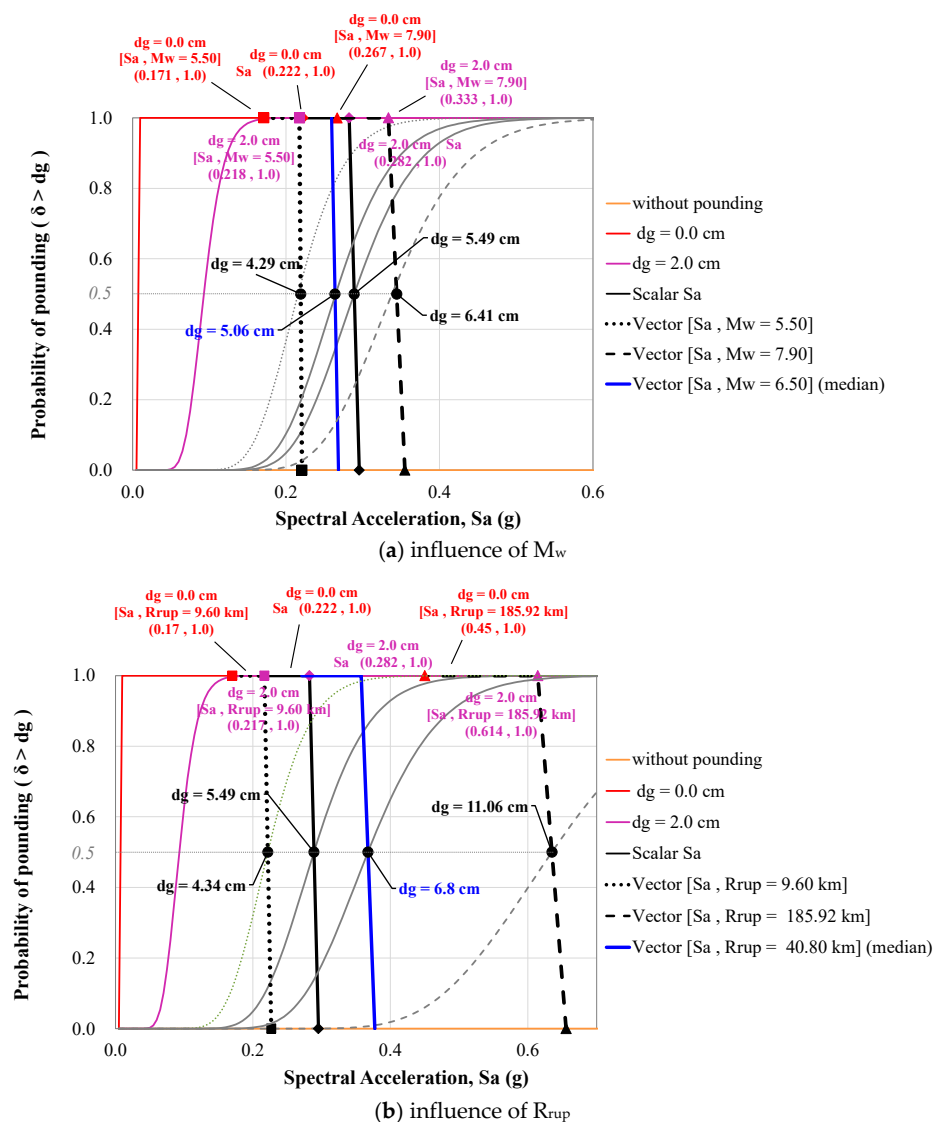


Figure 7. Influence of M_w and R_{rup} on the compounded fragility-based evaluation of the distance $d_{g,min}$ between the adjacent structures.

It can be observed that the variation in M_w and R_{rup} alters the performance level threshold and creates different solutions regarding the $d_{g,min}$ between the adjacent structures. For example, based on the scalar IM approach and considering that the probability of pounding is 50%, a separation gap distance approximately equal to 5.49 cm is required to ensure that the performance level of IO is not exceeded. For the same probability of pounding in the case of vector-valued $[S_{a,T1}, M_w]$, when $M_w = 7.90$ the corresponding minimum demand for d_g is equal to 6.41 cm. In the case of a vector-valued IM consisting of $S_{a,T1}$ and R_{rup} , when $R_{rup} = 9.6$ km the corresponding minimum demand for d_g is equal to 4.34 cm. However, the threshold line in the case of scalar intensity $S_{a,T1}$ provides a similar estimation for the minimum separation gap distance d_g as the one accomplished based on the vector-valued $S_{a,T1}$ conditional to median values of M_w and R_{rup} (Figure 7). The results for all the examined cases are presented in Figure 7. Based on these results, it can be noted that the predictive power of R_{rup} seems to be greater than M_w .

7. Conclusions

In this study, the effect of M_w and R_{rup} on the fragility assessment of an eight-story RC frame against floor-to-floor structural pounding conditions is estimated. In this way, initial results regarding the degree of bias induced on the fragility analyses due to ground motions'

uncertainties are introduced. Further, the predictive capability of the commonly used PGA and $S_{a,T1}$ is evaluated among other 21 scalar IMs. Finally, new PSDMs and fragility curves based on vector-valued IMs are presented and compared with the corresponding scalar-based fragilities. The results of this study highlight the following issues:

- The structural dependent IMs are more efficient in predicting the seismic demands of the eight-story RC structure. However, an optimal IM that simultaneously satisfies the criteria of efficiency and sufficiency is difficult to be defined. IMs' efficiency or sufficiency properties seem not to be affected when structural pounding is involved.
- The scalar IM of $S_{a,T1}$ passes the criteria of efficiency, while p -values are shifted close to 0.05 in all the examined cases. Also, based on the RSM method, the superiority of $S_{a,T1}$ among the other IMs is justified.
- The variation in M_w and R_{rup} alters the results of the assessment against structural pounding. Once M_w or R_{rup} is increased, fragility curves are shifted to greater values of IM, and the probability of exceedance of a certain performance level is reduced. Nevertheless, the variation in the results of the fragility analysis is more pronounced when R_{rup} is involved.
- The variation in M_w and R_{rup} generates different demand solutions for the adequate separation gap distance d_g between the adjacent structures, which in some cases also leads to premature exceedance of a certain capacity level of the structure.

In this study, the effect of M_w and R_{rup} was examined considering only the case of floor-to-floor structural pounding. Therefore, the critical shear performances of the structural members due to floor-to-column pounding conditions have not been addressed. An issue that also needs to be further investigated is the predictive capability of the established fragility curves against structural pounding when two or more scalar IMs are involved in the analysis process.

Author Contributions: Conceptualization, M.G.F. and M.J.F.; methodology, M.G.F. and M.J.F.; investigation, M.G.F.; writing—original draft preparation, M.G.F.; writing—review and editing, M.J.F. All authors have read and agreed to the published version of the manuscript.

Funding: This research was co-financed by Greece and the European Union (European Social Fund-ESF) through the Operational Programme «Human Resources Development, Education and Lifelong Learning» in the context of the Act “Enhancing Human Resources Research Potential by undertaking a Doctoral Research” Sub-action 2: IKY Scholarship Programme for PhD candidates in the Greek Universities.

Data Availability Statement: The data presented in this study are available on request from the corresponding author.

Conflicts of Interest: The authors declare no conflict of interest. The funders had no role in the design of the study; in the collection, analyses, or interpretation of data; in the writing of the manuscript; or in the decision to publish the results.

References

1. Flenga, M.G.; Favvata, M.J. Probabilistic seismic assessment of the pounding risk based on the local demands of a multistory RC frame structure. *Eng. Struct.* **2021**, *245*, 112789. [[CrossRef](#)]
2. Rayegani, A.; Nouri, G. Seismic collapse probability and life cycle cost assessment of isolated structures subjected to pounding with smart hybrid isolation system using a modified fuzzy based controller. *Structures* **2022**, *44*, 30–41. [[CrossRef](#)]
3. Cornell, C.A.; Jalayer, F.; Hamburger, R.O.; Foutch, D.A. Probabilistic Basis for 2000 SAC Federal Emergency Management Agency Steel Moment Frame Guidelines. *J. Struct. Eng.* **2002**, *128*, 526–533. [[CrossRef](#)]
4. Shome, N. Probabilistic Seismic Demand Analysis of Nonlinear Structures. Ph.D. Thesis, Department of Civil Engineering, Stanford University, Stanford, CA, USA, 1999.
5. Luco, N.; Cornell, C.A. Structure-specific scalar intensity measures for near-source and ordinary earthquake ground motions. *Earthq. Spectra* **2007**, *23*, 357–392. [[CrossRef](#)]
6. Padgett, J.E.; Nielson, B.G.; DesRoches, R. Selection of optimal intensity measures in probabilistic seismic demand models of highway bridge portfolios. *Earthq. Eng. Struct. Dyn.* **2008**, *37*, 711–725. [[CrossRef](#)]
7. Giovenale, P.; Cornell, C.A.; Esteva, L. Comparing the adequacy of alternative ground motion intensity measures for the estimation of structural responses. *Earthq. Eng. Struct. Dyn.* **2004**, *33*, 951–979. [[CrossRef](#)]

8. Ebrahimian, H.; Jalayer, F.; Lucchini, A.; Mollaioli, F.; Manfredi, G. Preliminary ranking of alternative scalar and vector intensity measures of ground shaking. *Bull. Earthq. Eng.* **2015**, *13*, 2805–2840. [[CrossRef](#)]
9. Mollaioli, F.; Lucchini, A.; Cheng, Y.; Monti, G. Intensity measures for the seismic response prediction of base-isolated buildings. *Bull. Earthq. Eng.* **2013**, *11*, 1841–1866. [[CrossRef](#)]
10. Kostinakis, K.; Athanatopoulou, A.; Morfidis, K. Correlation between ground motion intensity measures and seismic damage of 3D R/C buildings. *Eng. Struct.* **2014**, *82*, 151–167. [[CrossRef](#)]
11. Elenas, A.; Meskouris, K. Correlation study between seismic acceleration parameters and damage indices of structure. *Eng. Struct.* **2001**, *23*, 698–704. [[CrossRef](#)]
12. Tubaldi, E.; Freddi, F.; Barbato, M. Probabilistic seismic demand and fragility assessment for evaluating the separation distance between adjacent buildings. In Proceedings of the 11st International Conference on Structural Safety and Reliability (ICOSSAR 2013), New York, NY, USA, 16–20 June 2013; pp. 1–8.
13. Tubaldi, E.; Freddi, F.; Barbato, M. Probabilistic seismic demand model for pounding risk assessment. *Earthq. Eng. Struct. Dyn.* **2016**, *45*, 1743–1758. [[CrossRef](#)]
14. Flegga, M.G.; Favvata, M.J. Global and local performance levels on the probabilistic evaluation of the structural pounding effect between adjacent rc structures. In Proceedings of the 11st International conference on structural dynamics (EURODYN 2020), Athens, Greece, 23–26 November 2020; pp. 3762–3779.
15. Flenga, M.G.; Favvata, M.J. Fragility assessment of the inter-story pounding risk between adjacent reinforced concrete structures based on probabilistic seismic demand models. In Proceedings of the 13th International Conference on Earthquake Resistant Engineering Structures (ERES 2021), Online, 26–28 May 2021; pp. 3–13.
16. Flenga, M.G.; Favvata, M.J. Fragility Curves and Probabilistic Seismic Demand Models on the Seismic Assessment of RC Frames Subjected to Structural Pounding. *Appl. Sci.* **2021**, *11*, 8253. [[CrossRef](#)]
17. Langlade, T.; Bertrand, D.; Grange, S.; Candia, G.; Llera, J. Intensity measures properties and selection for risk analysis on structures subjected to earthquake induced building pounding with a non-smooth contact dynamics method. In Proceedings of the 8th ECCOMAS Thematic Conference on Computational Methods in Structural Dynamics and Earthquake Engineering (COMPDYN 2021), Athens, Greece, 28–30 June 2021; pp. 4621–4632.
18. Nazri, F.M.; Miari, M.; Kassem, M.M.; Tan, C.G.; Farsangi, E.N. Probabilistic Evaluation of Structural Pounding Between Adjacent Buildings Subjected to Repeated Seismic Excitations. *Arab. J. Sci. Eng.* **2018**, *44*, 4931–4945. [[CrossRef](#)]
19. Kazemi, F.; Miari, M.; Jankowski, R. Investigating the effects of structural pounding on the seismic performance of adjacent RC and steel MRFs. *Bull. Earthq. Eng.* **2021**, *19*, 317–343. [[CrossRef](#)]
20. Baker, J.W.; Cornell, C.A. A vector-valued ground motion intensity measure consisting of spectral acceleration and epsilon. *Earthq. Eng. Struct. Dyn.* **2005**, *34*, 1193–1217. [[CrossRef](#)]
21. Baker, J.W. Probabilistic structural response assessment using vector-valued intensity measures. *Earthq. Eng. Struct. Dyn.* **2007**, *36*, 1861–1883. [[CrossRef](#)]
22. Alembagheri, M. Investigating efficiency of vector-valued intensity measures in seismic demand assessment of concrete dams. *Adv. Civ. Eng.* **2018**, *2018*, 5675032. [[CrossRef](#)]
23. Chen, X.; Xiang, N.; Guan, Z.; Li, J. Seismic vulnerability assessment of tall pier bridges under mainshock-aftershock-like earthquake sequences using vector-valued intensity measure. *Eng. Struct.* **2022**, *253*, 113732. [[CrossRef](#)]
24. Saha, A.; Mishra, S.K. Synthesis of a vector-valued intensity measure for improved prediction of seismic demands in Inter-Story-Isolated (ISI) buildings subjected to near fault ground motions. *Eng. Struct.* **2021**, *248*, 113241. [[CrossRef](#)]
25. Sun, B.; Zhang, G.; Xue, B.; Kou, L.; Hu, L.; Liu, W. The analysis of the optimal scalar and vector intensity measurements for seismic performance assessment of deep-buried hydraulic arched tunnels. *Undergr. Space* **2023**, *9*, 218–233. [[CrossRef](#)]
26. Favvata, M.J. Minimum required separation gap for adjacent RC frames with potential inter-story seismic pounding. *Eng. Struct.* **2017**, *152*, 643–659. [[CrossRef](#)]
27. Prakash, V.; Powell, G.H.; Gampbell, S. *DRAIN-2DX Base Program Description and User's Guide, UCB/SEMM*; Report No. 17/93; University of California: Orkland, CA, USA, 1993.
28. PEER Ground Motion Database. 2011. Available online: <https://peer.berkeley.edu/peer-strong-ground-motion-databases> (accessed on 10 October 2017).
29. ESM Database. Available online: <https://esm-db.eu/#/home> (accessed on 20 April 2020).
30. Rayegani, A.; Nouri, G. Application of smart dampers for prevention of seismic pounding in isolated structures subjected to near-fault earthquakes. *J. Earthq. Eng.* **2022**, *26*, 4069–4084. [[CrossRef](#)]
31. Kramer, S.L. *Geotechnical Earthquake Engineering*, 1st ed.; Prentice Hall: Upper Saddle River, NJ, USA, 1996.
32. Reed, J.W.; Anderson, N.; Chokshi, N.C.; Kennedy, R.P.; Metevia, W.J.; Ostrom, D.K.; Stevenson, J.D. *A Criterion for Determining Exceedance of the Operating Basis Earthquake*; EPRI Report NP-5930; Electric Power Research Institute: Palo Alto, CA, USA, 1988; Volume 18, pp. 805–810.
33. Nuttli, O.W. *The Relation of Sustained Maximum Ground Acceleration and Velocity to Earthquake Intensity and Magnitude*; Paper S-71-1, Report 16; U.S. Army Corps of Engineers, Waterways Experiment Station: Vicksburg, MS, USA, 1979.
34. Housner, G.W.; Jennings, P.C. Generation of Artificial Earthquakes. *ASCE J. Eng. Mech.* **1964**, *90*, 113–150. [[CrossRef](#)]
35. Arias, A. Arias, A. A measure of earthquake intensity. In *Seismic Design for Nuclear Power Plants*; Hansen, R.J., Ed.; MIT Press: Cambridge MA, USA, 1970; pp. 438–483.

36. Park, Y.J.; Ang, A.H.S.; Wen, Y.K. Seismic damage analysis of reinforced concrete buildings. *ASCE J. Struct. Eng.* **1985**, *111*, 740–757. [[CrossRef](#)]
37. Anderson, J.C.; Bertero, V.V. Uncertainties in Establishing Design Earthquakes. *ASCE J. Struct. Eng.* **1987**, *113*, 1709–1724. [[CrossRef](#)]
38. Sarma, S.K.; Yang, K.S. An evaluation of strong motion records and a new parameter A95. *Earthq. Eng. Struct. Dyn.* **1987**, *15*, 119–132. [[CrossRef](#)]
39. Von Thun, J.L.; Rochim, L.H.; Scott, G.A.; Wilson, J.A. Earthquake ground motions for design and analysis of dams. In *Earthquake Engineering and Soil Dynamics II—Recent Advances in Ground-Motion Evaluation*. In Proceedings of the Specialty Conference, Park City, UT, USA, 27–30 June 1988; Volume 20, pp. 463–481.
40. Dimitrakopoulos, E.; Kappos, A.; Makris, N. Dimensional analysis of yielding and pounding structures for records without distinct pulses. *Soil Dyn. Earthq. Eng.* **2009**, *29*, 1170–1180. [[CrossRef](#)]
41. Housner, G.W. *Spectrum Intensities of Strong Motion Earthquakes*; Symposium on Earthquake and Blast Effects on Structures: Los Angeles, CA, USA, 1952.
42. Bianchini, M.; Diotallevi, P.P.; Baker, J.W. Prediction of Inelastic Structural Response Using an Average of Spectral Accelerations. In Proceedings of the 10th International Conference on Structural Safety and Reliability (ICOSSAR 2009), Osaka, Japan, 13–17 September 2009; pp. 1–8.
43. Jalayer, F.; Beck, J.; Zareian, F. Analyzing the Sufficiency of Alternative Scalar and Vector Intensity Measures of Ground Shaking Based on Information Theory. *ASCE J. Eng. Mech.* **2012**, *138*, 307–316. [[CrossRef](#)]

Disclaimer/Publisher’s Note: The statements, opinions and data contained in all publications are solely those of the individual author(s) and contributor(s) and not of MDPI and/or the editor(s). MDPI and/or the editor(s) disclaim responsibility for any injury to people or property resulting from any ideas, methods, instructions or products referred to in the content.